Characterization and Control of Biological Microrobots

Islam S. M. Khalil, Marc P. Pichel, Lars Zondervan, Leon Abelmann and Sarthak Misra

Abstract This work addresses the characterization and control of Magnetotactic Bacterium (MTB) which can be considered as a biological microrobot. Magnetic dipole moment of the MTB and response to a field-with-alternating-direction are characterized. First, the magnetic dipole moment is characterized using four techniques, i.e., Transmission Electron Microscope images, *flip-time*, *rotating-field* and *u-turn* techniques. This characterization results in an average magnetic dipole moment of 3.32×10^{-16} A.m^2 and 3.72×10^{-16} A.m^2 for non-motile and motile MTB, respectively. Second, the frequency response analysis of MTB shows that its velocity decreases by 38% for a field-with-alternating-direction of 30 rad/s. Based on the characterized magnetic dipole moment, the magnetic force produced by our magnetic system is five orders-of-magnitude less than the propulsion force generated by the flagellum of the MTB. Therefore, *point-to-point* positioning of MTB cannot be achieved by exerting a magnetic force. A closed-loop control strategy is devised based on calculating the position tracking error, and capitalizes on the frequency response analysis of the MTB. *Point-to-point* closed-loop control of MTB is achieved for a reference set-point of 60 μm with average velocity of 20 μm/s. The closed-loop control system positions the MTB within a region-of-convergence of 10 μm diameter.

Islam S. M. Khalil, Marc P. Pichel and Sarthak Misra
MIRA–Institute for Biomedical Technology and Technical Medicine, University of Twente, 7500 AE Enschede, The Netherlands.
e-mail: i.s.m.khalil@utwente.nl

Lars Zondervan and Leon Abelmann
MESA+ Institute for Nanotechnology, University of Twente, 7500 AE Enschede, The Netherlands.

1 Introduction

Recently, considerable progress has been made in the area of medical microrobots, with dimensions in the range of 100 μm or less [1]. These microrobots have the potential to perform targeted drug delivery and actuation of micro-objects [2, 3]. Two strategies are being proposed for propulsion: extracting energy from an external magnetic field [4], or extracting energy from the surrounding liquid and using the external magnetic field for steering only [5]. In the latter case, control of the microrobot is a challenge and to study this control issue, we benefit from Magnetotactic Bacterium (MTB), which uses the earth's magnetic field to orient itself [6, 7]. MTB contains magnetic nano-crystals enveloped by an organic membrane as shown in Fig. 1. These nano-crystals are arranged as a chain along the longitudinal axis of the MTB and provide a magnetic dipole moment which enables the MTB to passively orient itself along the magnetic field lines [8]. Often MTB, which can be considered as a biological microrobot, possesses flagella at its ends which provide self-propulsion along the field lines. Therefore, MTB or a swarm of magnetotactic bacteria can be utilized to transport and steer micro-objects using the forces generated by the flagella and the torque exerted on the magnetic nano-crystal chain, respectively [9]. However, due to limitations on generating relatively large field gradients, velocity of the MTB cannot be controlled and its closed-loop control cannot be achieved by pulling the MTB using field gradients [10]. Therefore, a frequency response-based closed-loop control strategy is presented to control the MTB without relatively large field gradients.

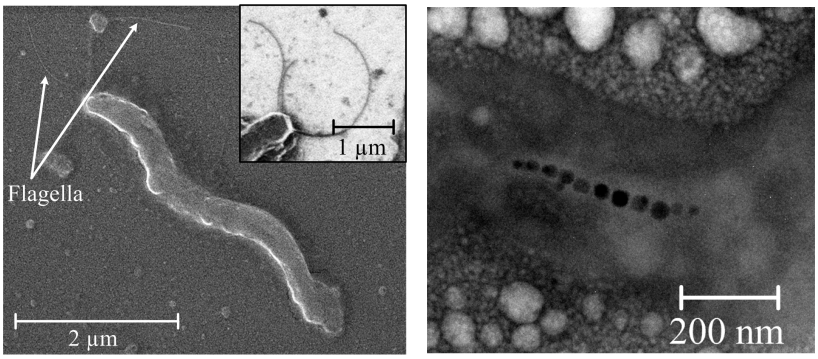

(a) Magnetotactic Bacterium (b) Magnetite nano-crystals

Fig. 1 Scanning/Transmission Electron Microscope (SEM/TEM) images of the Magnetotactic Bacterium (MTB), i.e., *Magnetospirillum magnetotacticum* (MS-1). (a) SEM image of the MTB. MTB propels itself by rotating its helical flagella. The flagella are illustrated by the inset taken by a SEM. (b) TEM image of a chain of magnetite nano-crystals. The nano-crystal chain is enveloped by an organic membrane and the interaction between the magnetic dipole moment and the external field allows the MTB to be oriented along the field lines. The nano-crystals have a cuboctahedral morphology and an edge length of $\sim$ 36 nm.

In this work, we characterize the magnetic dipole moment and the frequency response of MTB. First, magnetic dipole moment of MTB is characterized using its TEM images. The *flip-time* of non-motile MTB during field reversal is used to characterize its magnetic dipole moment. In addition, based on motion analysis, the magnetic dipole moment of motile MTB is estimated by analyzing its behavior under the influence of rotating fields and field reversals [11,12]. Second, response of the MTB to a field-with-alternating-direction is investigated and provides a strategy to perturb the vibrational and rotational modes of its flagella, hence decreasing its velocity. The estimated magnetic dipole moment is used in the realization of the magnetic torque-current map, which is necessary for the open-loop control system. Furthermore, the force-current map is utilized along with the frequency response of the MTB to realize the closed-loop control system.

The remainder of this paper is organized as follows: In Section 2 we shall discuss the theoretical background pertaining to the general characterization of the magnetic dipole moment of MTB using non-motile techniques (TEM images and *flip-time*) and motile techniques which depends on motion analysis (*rotating-field* and *u-turn*). In addition, frequency response of MTB is characterized. Open- and closed-loop control strategies of MTB are analyzed in Section 3. Discussion about the presented control strategies, characterization techniques, directions for future work and conclusions are provided in Section 4.

2 Characterization of Magnetotactic Bacterium

Under the influence of a magnetic field, the magnetic torque $\left(\mathbf{T}(\mathbf{P}) \in \mathbb{R}^{3\times 1}\right)$ and force $\left(\mathbf{F}(\mathbf{P}) \in \mathbb{R}^{3\times 1}\right)$ experienced by a MTB located at position $\left(\mathbf{P} \in \mathbb{R}^{3\times 1}\right)$ are given by

$$\mathbf{T}(\mathbf{P}) = \mathbf{m} \times \mathbf{B}(\mathbf{P}) \text{ and } \mathbf{F}(\mathbf{P}) = (\mathbf{m} \cdot \nabla)\mathbf{B}(\mathbf{P}), \tag{1}$$

where $\mathbf{m} \in \mathbb{R}^{3\times 1}$ and $\mathbf{B}(\mathbf{P}) \in \mathbb{R}^{3\times 1}$ are the magnetic dipole moment of the MTB and the induced magnetic field, respectively. The flagellum of the MTB is modeled as a helical propeller with length, thickness, diameter (of the MTB) and pitch of 12 μm, 20 nm, 0.5 μm and 2 μm, respectively. The propulsion force generated by this helical propeller is calculated by a model provided in [13], and results in 2×10^{-12} N at linear velocity of 20 μm/s. In order to determine the magnetic torque and force, we have to estimate the magnetic dipole moment of the MTB.

2.1 Magnetic dipole moment characterization

TEM images can be used to determine the magnetic dipole moment of motile and non-motile MTB. The *flip-time* technique allows for calculating the magnetic dipole

moment of non-motile MTB, whereas the *rotating-field* and the *u-turn* techniques provide magnetic dipole moment of motile MTB based on its motion analysis.

2.1.1 Transmission electron microscope images

The TEM image of the MTB indicates that a nano-crystal chain is fixed in its organic membrane as shown in Fig. 1(b). These nano-crystals have a cuboctahedral morphology. Using the number of nano-crystals and the cuboctahedron edge length ($\sim$ 36 nm), the magnetic dipole moment has an upper limit given by

$$\mid \mathbf{m} \mid = \sum_{i=1}^{k} \mathrm{M_s V}_i, \tag{2}$$

where $\mathrm{M_s}$ is the saturation magnetization of magnetite (4.3×10^5 A.m^{-1}). Further, k and V_i are the number and volume of the ith magnetite nano-crystal, respectively.

2.1.2 *Flip-time* technique

Non-motile MTB undergoes flip turn when the magnetic field is reversed. The elapsed-time of the flip turn (τ), i.e., *flip-time*, is given by

$$\tau = \frac{\alpha}{\mid \mathbf{m} \mid\mid \mathbf{B}(\mathbf{P}) \mid} \ln\left(\frac{2 \mid \mathbf{m} \mid\mid \mathbf{B}(\mathbf{P}) \mid}{\mathrm{k}T}\right), \tag{3}$$

where k and T are the Boltzmann constant and the temperature of the medium in which MTB navigates, respectively [11]. Further, α is the rotational drag coefficient given by

$$\alpha = \frac{\pi \eta L^3}{3}\left[\ln\left(\frac{L}{d}\right) + 0.92\left(\frac{d}{L}\right) - 0.662\right]^{-1}, \tag{4}$$

where η is the medium dynamic viscosity. Further, L and d are the length and diameter of the MTB, respectively [14]. The *flip-time* can be determined experimentally, then the magnetic dipole moment can be calculated by solving (3).

2.1.3 *Rotating-field* technique

Under the influence of a rotating magnetic field [17], the relation between the magnetic torque and the angular velocity of the MTB (ω) is

$$\mid \mathbf{m} \mid\mid \mathbf{B}(\mathbf{P}) \mid \sin\beta + \alpha\omega = 0, \tag{5}$$

where β is the angle between the induced magnetization field and the magnetic dipole moment. Characterization of the magnetic dipole moment requires determi-

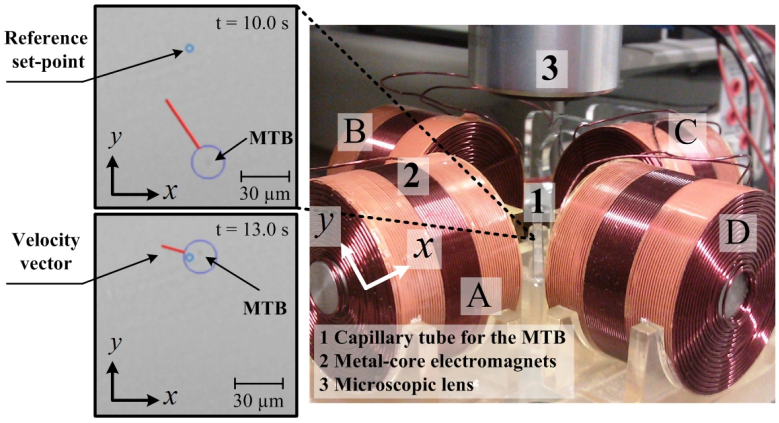

Fig. 2 Magnetic system developed for characterization and control of Magnetotactic Bacterium (MTB) by the magnetic fields generated at each of the electromagnets. The system consists of a microscope equipped with a vision system mounted on the top of an array of electromagnets surrounding a flat capillary tube which incubates a culture of magnetotactic bacteria [15]. The capillary tube has an inner thickness, an inner width and length of 0.2 mm, 2 mm and 50 mm, respectively (VitroCom, VitroTubes 3520-050, Germany). The insets show a closed-loop controlled MTB (tracked and marked by the large blue circle) moving towards a reference set-point by the magnetic fields and its self-propulsion. The electromagnets are labeled with the letters A, B, C and D.

nation of its boundary frequency (ω_b). This frequency can be determined by gradually increasing the frequency of the rotating field and observing the frequency after which MTB can no longer follow the field, i.e., $\omega = \omega_b$, when $\sin\beta = 1$. Therefore, (5) can be written as

$$| \mathbf{m} || \mathbf{B}(\mathbf{P}) | + \alpha\omega_b = 0, \tag{6}$$

The boundary frequency can be determined experimentally and used in (6) to calculate the magnetic dipole moment.

2.1.4 *U-turn* technique

Under magnetic field reversals, MTB undergoes u-turn trajectories [11]. The u-turn diameter (D) is given by

$$D = \frac{\alpha\pi v}{| \mathbf{m} || \mathbf{B}(\mathbf{P}) |}, \tag{7}$$

where v is the linear velocity of the MTB. The u-turn diameter can be determined experimentally and used in (7) to calculate the magnetic dipole moment. It is worth noting that (3) represents the u-turn elapsed-time for motile MTB. The elapsed-time can be determined and used in (3) to calculate the magnetic dipole moment.

2.2 Frequency response characterization

Velocity of the MTB depends on the rotational and vibrational modes of its flagella. Our MTB, i.e., *Magnetospirillum magnetotacticum* (MS-1), provides propulsion by rotating its helical flagella at ∼628.3 rad/s [14]. Alternating the direction of the field lines could perturb the desirable modes of the MTB, and hence decreases its velocity. This allows for devising a closed-loop control strategy which is partially based on alternating the direction of the field to decrease the velocity of the MTB.

2.3 Characterization results

Characterization of the magnetic dipole moment is conducted on a magnetic system with four orthogonal metal-core electromagnets. The system is capable of providing magnetic fields and field gradients of 15 mT and 60 mT/m, respectively [15]. The electromagnets array surrounds a capillary tube as shown in Fig. 2. The capillary tube incubates a culture of magnetotactic bacteria in 0.02 ml of growth medium. The bacterial density ranges from 10^6/ml to 10^7/ml. The *Magnetospirillum magnetotacticum* (MS-1) cultures utilized in our work are grown according to the protocol provided in Bertani *et al.* [16].

First, the TEM images of 15 magnetotactic bacteria are used to determine the number and volume of the magnetite nano-crystals illustrated in Fig. 1(b). The calculated magnetic dipole moment using (2), has an average of 3.0×10^{-16} A.m^2.

MTB undergoes flip-turns during field reversals, The *flip-time* is determined experimentally and used in (3) to calculate the magnetic dipole moment. An electromagnet (electromagnet D in Fig. 2) is utilized to generate uniform magnetic field of 7.9 mT. The *flip-time* is calculated from the initiation time of the field reversal until MTB completes a 180 degrees turn. The field reversal is initiated in the first frame of

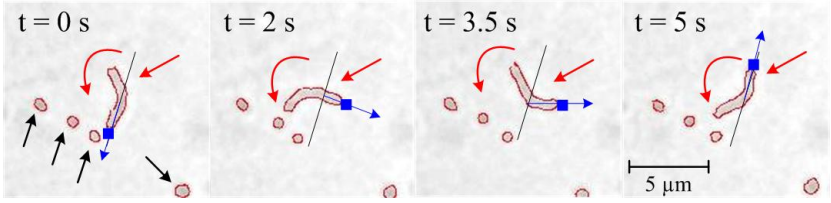

Fig. 3 Non-motile Magnetotactic Bacterium (MTB) undergoing counter-clockwise flip turn when it is subjected to magnetic field reversal. The red arrow indicates the flipping MTB, whereas the black arrows indicate non-flipping and non-motile magnetotactic bacteria in its vicinity. The curved red arrow indicates the direction of rotation. The blue mark indicates one end of the MTB. The MTB changes the curvature of its membrane while its rotating, as shown in the second and third frames. The magnetic dipole moment is calculated for 15 magnetotactic bacteria, and results in an average of 3.32×10^{-17} A.m^2 for magnetic field and average *flip-time* of 7.9 mT and 5.8 s, respectively. Magnetic dipole moment is calculated using (3).

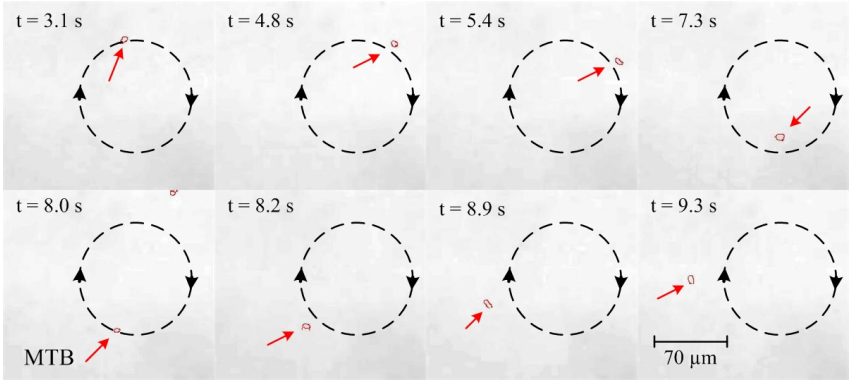

Fig. 4 Motion of the Magnetotactic Bacterium (MTB) under the influence of a rotating magnetic field with gradually increasing frequency from 1 rad/s to 10 rad/s. The black-dashed circle illustrates the path and direction of the MTB. The red arrow indicates the MTB. The images are processed to detect the edges of the MTB. As we gradually increase the rotating field frequency, the MTB can no longer follow the fields, as shown in the last frame of the top row at, t = 7.3 s and field frequency of 9.5 rad/s. The estimated magnetic dipole moment using the *rotating-field* technique is 4.34×10^{-16} A.m^2 at magnetic field of 7.9 mT and boundary frequency of 9.5 rad/s. Magnetic dipole moment is calculated using (6).

Fig. 3, and the non-motile MTB completes a 180 degrees turn in 5 s. The *flip-time* is used in (3) to calculate the magnetic dipole moment for 15 magnetotactic bacteria, and results in an average of 3.32×10^{-16} A.m^2.

In order to determine the magnetic dipole moment of motile MTB using the *rotating-field* technique, two orthogonal electromagnets (electromagnets A and D) are used to generate rotating fields at 7.9 mT. The MTB follows the rotating fields up to a specific frequency (the boundary frequency) after which it can no longer follow the fields, and deviates from its circular trajectory. The frequency of the applied rotating field is increased gradually from 1 rad/s to 10 rad/s. We observed from the off-line motion analysis that MTB has boundary frequency of 9.5 rad/s as shown in the last frame of the top row of Fig. 4. The length and diameter of the MTB are determined by the TEM image of Fig. 1(a), and used along with the boundary frequency (ω_b) to calculate the magnetic dipole moment using (4) and (6). The average magnetic dipole moment is 4.34×10^{-16} A.m^2 for 15 magnetotactic bacteria.

Magnetic dipole moment of motile MTB is determined using the *u-turn* technique. An electromagnet (electromagnet A) is used to generate magnetic field of 7.9 mT. The MTB undergoes u-turn trajectory when the field is reversed as shown in Fig. 5. The u-turn diameter is determined from the off-line motion analysis of the u-turn trajectory. Using (7), the average magnetic dipole moment is 3.11×10^{-16} A.m^2 for 15 magnetotactic bacteria. Results of the magnetic dipole moment characterization are summarized in Table 1.

A magnetic field-with-alternating-direction is applied to investigate the effect of the field frequency on the velocity of the MTB. The frequency of the applied field is gradually increased from 1 rad/s to 30 rad/s, then the velocity is measured at each

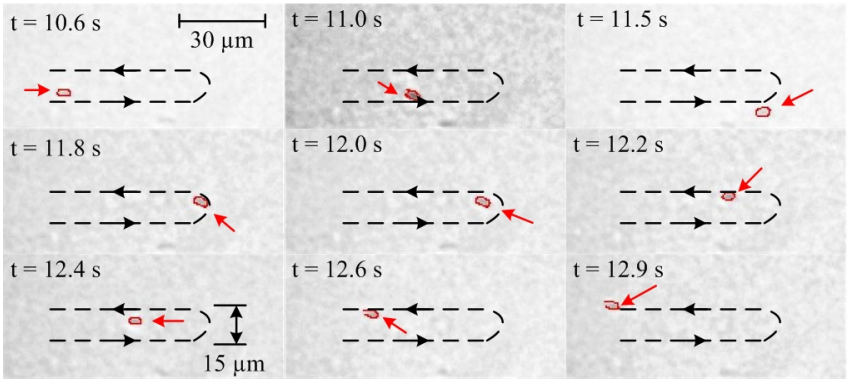

Fig. 5 Motion of the Magnetotactic Bacterium (MTB) during magnetic field reversal. The MTB (length$\sim$5 μm) performs a u-turn trajectory marked with the black dashed line, during the field reversal. The red arrow indicates the MTB. The u-turn diameter ($\sim$15 μm) is used to estimate the MTB magnetic dipole moment. The elapsed-time can be determined starting from the field reversal initiation time until the MTB aligns itself along the field lines. The average magnetic dipole moment for 15 magnetotactic bacteria is 3.11×10^{-16} A.m^2 at magnetic field of 7.9 mT. Magnetic dipole moment is calculated using (7).

frequency for 15 magnetotactic bacteria. The frequency response experiment is conducted using two metal-core electromagnets (electromagnets B and D). Sinusoidal current inputs are simultaneously supplied at each of the electromagnets. Linearity of the current-field map ensures that the generated magnetic fields have the same frequency of the applied currents as shown in Fig. 6(a). Increasing the field frequency affects the velocity of the MTB as shown in Fig. 6(b). The average velocity of the MTB is decreased by 38% at field frequency of 30 rad/s.

Table 1 Characterized magnetic dipole moment by the Transmission Electron Microscope (TEM) images, *flip-time*, *rotating-field* and *u-turn* techniques. The average magnetic dipole moment represents the culture which includes both non-motile and motile magnetotactic bacteria. The average is calculated for 15 magnetotactic bacteria and from 15 TEM images.

Applied field magnitude	7.9 mT
Average magnetic dipole moment calculated from the TEM images	3.00×10^{-16} A.m^2
Average magnetic dipole moment - *flip-time* technique	3.32×10^{-16} A.m^2
Average magnetic dipole moment - *rotating-field* technique	4.34×10^{-16} A.m^2
Average magnetic dipole moment - *u-turn* technique	3.11×10^{-16} A.m^2

3 Control of Magnetotactic Bacterium

MTB can be oriented towards a desired trajectory using the following torque-current or field-current maps:

$$\mathbf{T}(\mathbf{P}) = \widehat{\mathbf{m}}\widetilde{\mathbf{B}}(\mathbf{P})\mathbf{I} \text{ and } \mathbf{B}(\mathbf{P}) = \widetilde{\mathbf{B}}(\mathbf{P})\mathbf{I}, \tag{8}$$

where $\mathbf{I} \in \mathbb{R}^{n\times 1}$ is a vector of the current inputs at each of the n-electromagnets. Further, $\widehat{\cdot}$ is the cross-product operator (3×3 skew-symmetric matrix). The input current vector is mapped onto magnetic field by the matrix ($\widetilde{\mathbf{B}}(\mathbf{P}) \in \mathbb{R}^{3\times n}$). The magnetic force can be represented by

$$\mathbf{F}(\mathbf{P}) = \left[\frac{\partial \mathbf{B}(\mathbf{P})}{\partial x}\frac{\partial \mathbf{B}(\mathbf{P})}{\partial y}\frac{\partial \mathbf{B}(\mathbf{P})}{\partial z}\right]^{\mathrm{T}}\mathbf{m} = \left[\frac{\partial \widetilde{\mathbf{B}}(\mathbf{P})\mathbf{I}}{\partial x}\frac{\partial \widetilde{\mathbf{B}}(\mathbf{P})\mathbf{I}}{\partial y}\frac{\partial \widetilde{\mathbf{B}}(\mathbf{P})\mathbf{I}}{\partial z}\right]^{\mathrm{T}}\mathbf{m}. \tag{9}$$

Using (8), MTB will perform flagellated swim along the field lines, this is sufficient to realize the open-loop control system. However, to realize the closed-loop control system, we calculate the position and velocity tracking errors along x- and y-axis,

$$\mathbf{e} = \mathbf{P}_{ref} - \mathbf{P} \text{ and } \dot{\mathbf{e}} = \dot{\mathbf{P}}_{ref} - \dot{\mathbf{P}}, \tag{10}$$

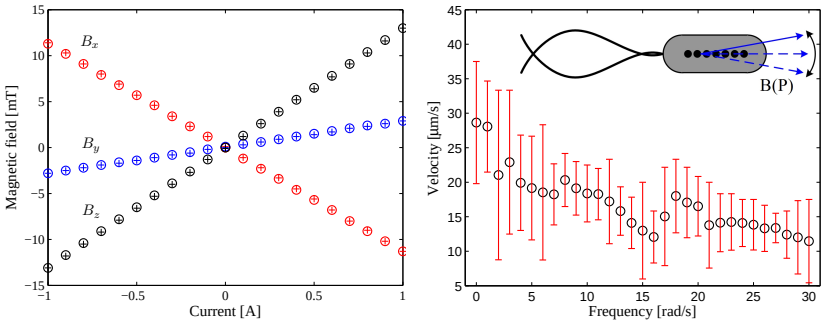

(a) Field-current linearity (b) Frequency response

Fig. 6 Frequency response analysis of Magnetotactic Bacterium (MTB). (a) Experimental validation of the current-magnetic field linearity and hysteresis. Magnetic field components at a representative point (10 mm along the centerline and from the side of electromagnet A) within the system's workspace (50 mm $\times$ 2 mm $\times$ 0.2 mm) are plotted versus the increasing (denoted by $\circ$) and decreasing (denoted by $+$) currents. The red, blue and black colors represent the magnetic field components (B_x, B_y and B_z) along x-, y- and z-axis, respectively. The fields are measured by a calibrated three-axis Hall magnetometer (Sentron AG, Digital Teslameter 3MS1-A2D3-2-2T, Switzerland). (b) Velocity of MTB versus the field frequency. The velocity is measured for 15 magnetotactic bacteria at each field frequency. The black circles represent the average velocity of the MTB, whereas the red bars represent the velocity error. Magnetic field-with-alternating-direction of frequency ranging from 1 rad/s to 30 rad/s is generated (represented by the blue solid and dashed arrows in the inset) by two metal-core electromagnets (B and D) at a magnetic field of 4 mT.

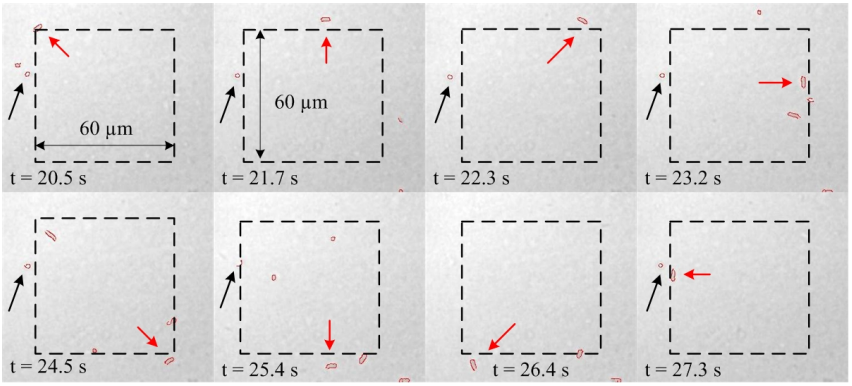

Fig. 7 Experimental open-loop control result of the Magnetotactic Bacterium (MTB). The red arrow indicates the position of the controlled MTB. The square trajectory illustrated with dashed black lines represents the reference trajectory (length $\sim$60 μm). The black arrow shows a non-motile MTB. The average velocity of the MTB during this trajectory is 32 μm/s.

where $\mathbf{e}$ and $\dot{\mathbf{e}}$ are the position and velocity tracking errors, respectively. Further, $\mathbf{P}_{ref}$ is a reference set-point. The desired force $(\mathbf{F}_{des}(\mathbf{P}))$ can be calculated by

$$\mathbf{F}_{des}(\mathbf{P}) = \mathbf{K}_1\mathbf{e} + \mathbf{K}_2\dot{\mathbf{e}}, \tag{11}$$

where $\mathbf{K}_1$ and $\mathbf{K}_2$ are the controller positive definite gain matrices. The desired force $(\mathbf{F}_{des}(\mathbf{P}))$ is provided by solving (9) for the current ($\mathbf{I}$) for each of the electromagnets [2]. The control law (11) will locate the MTB within the vicinity of the reference set-point, i.e., region-of-convergence.

Open-loop control is achieved experimentally by controlling the fields using (8), while closed-loop control is achieved by using (9), (10) and (11). In order to examine the effect of the field-with-alternating-direction on the velocity of the controlled MTB, closed-loop control experiments are conducted in the presence and absence of this field. In each case, velocity of the MTB and the size of the region-of-convergence are evaluated.

3.1 Open-loop control

In order to examine the open-loop control of MTB, we devised five trajectories, namely square, rectangular, u-turn, circular and figure-eight trajectories. Experimental result of the square trajectory is illustrated in Fig. 7, where MTB tracks a square trajectory of 60 μm length. In this experiment, the field lines are oriented towards the square trajectory coordinates. As soon as one or more magnetotactic bacteria approach the square coordinates, uniform fields are generated parallel to the trajectory by a single electromagnet at a time. The average velocity of the MTB

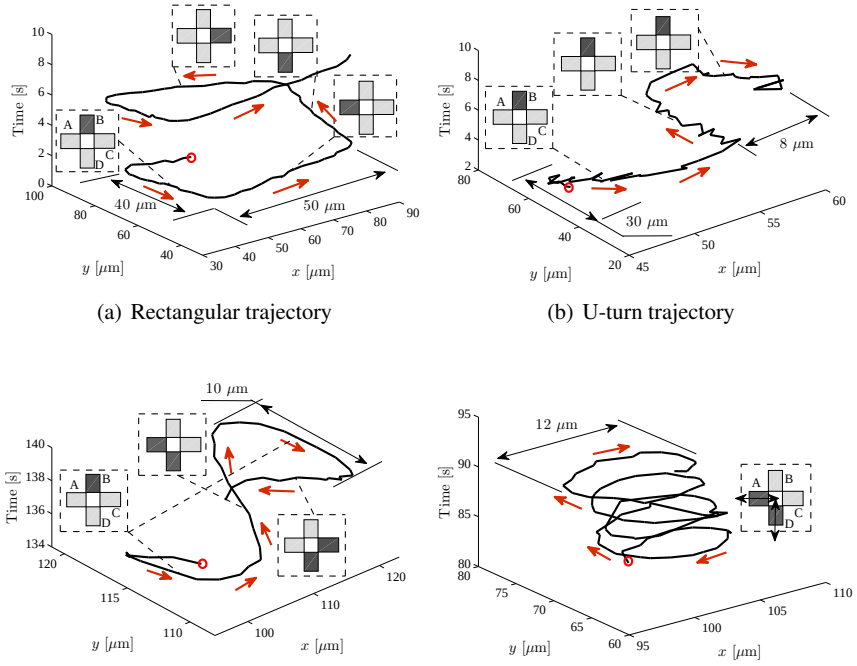

(a) Rectangular trajectory (b) U-turn trajectory

(c) Figure-eight trajectory (d) Circular trajectory

Fig. 8 Open-loop control of the Magnetotactic Bacterium (MTB) under the influence of magnetic fields. The black line represents the actual trajectory taken by the MTB, whereas the red arrows represent its direction. The red circle indicates the starting position and time of the trajectory. The insets indicate the active electromagnets (darker shade) that are synchronized by the open-loop control system to generate the necessary fields. (a) MTB follows a rectangular trajectory of 40 μm width and 50 μm length at average velocity of 36 μm/s. (b) MTB follows u-turn trajectory of 30 μm length and 8 μm diameter at average velocity of 17 μm/s. (c) MTB follows figure-eight trajectory of 25 μm length at average velocity of 23 μm/s. (d) MTB follows a circular trajectory of 12 μm diameter at average velocity of 28 μm/s. Electromagnets A and D provide sinusoidal fields illustrated with the black arrows.

is 32 μm/s. It is important to note that the field strength does not have any affect on the velocity of the MTB. Similarly, a MTB is controlled to follow a rectangular trajectory of 40 μm width and 50 μm length as shown in Fig. 8(a), at average velocity of 36 μm/s. Experimental result of the u-turn trajectory of 30 μm length and 8 μm diameter is illustrated in Fig. 8(b), at average velocity of 17 μm/s. Fig. 8(c) illustrates the experimental result of tracking figure-eight trajectory of 25 μm length at average velocity of 23 μm/s. Similarly, Fig. 8(d) illustrates the tracking result of a circular trajectory of 12 μm diameter at average velocity of 28 μm/s. The insets included in Fig. 8 indicate the active (darker shade) electromagnets of the system.

3.2 Closed-loop control

In order to examine the frequency response-based closed-loop control strategy, we investigate the *point-to-point* positioning of motile MTB in the presence and absence of a field-with-alternating-direction. Position and velocity tracking errors along x- and y-axis are calculated using (10). These errors are used to direct the fields towards the reference set-point using (9) and (11). First, $(\mathbf{F}_{des}(\mathbf{P}))$ is calculated based on the tracking error (10), then used in (9) along with the characterized magnetic dipole moment (4.34×10^{-16} A.m^2) to solve for the currents for each of the electromagnets. Field-with-alternating-direction at frequency of 30 rad/s is applied along with the fields generated using (11). The closed-loop control enforces the MTB to stay within the vicinity of the reference set-point. The trajectory taken by the MTB towards a reference set-point is shown in Fig. 9(a). The inset in Fig. 9(b) shows the response of the MTB within the vicinity of the reference set-point. The closed-loop control system enforces the MTB to stay within the vicinity of the reference set-point. The average velocity of the MTB during this experiment is 20 μm/s and the region-of-convergence has 10 μm diameter.

Closed-loop control is performed in the absence of the field-with-alternating-direction. Multiple reference set-points are tracked as shown in Figs. 10(a) and (b), with average velocity of 29 μm/s. This result indicates the effect of the field-with-alternating-direction on the velocity of the MTB. The two insets in Fig. 10(b) illustrate the effect of the closed-loop control on the behavior of the MTB. Due to

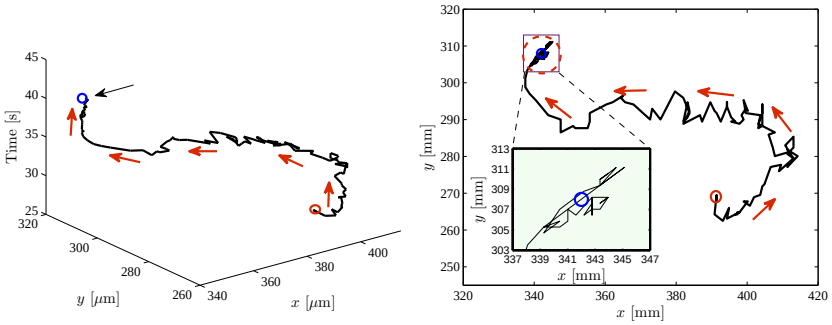

(a) Closed-loop tracking (b) MTB path

Fig. 9 Closed-loop control of the Magnetotactic Bacterium (MTB) under the influence of the magnetic fields in the presence of field-with-alternating-direction at frequency of 30 rad/s. The black line represents the actual trajectory taken by the MTB, whereas the red arrows represent its direction. The red and blue circles indicate the starting position and the reference set-point, respectively. The entries of the diagonal controller gain matrices ($\mathbf{K}_1$) and ($\mathbf{K}_2$) are 15.0 and 15.5, respectively. (a) Motion of the MTB towards a reference set-point (indicated by the black arrow). (b) The inset indicates the effect of the closed-loop control on the motion of the MTB at the reference set-point. The average velocity of the MTB is 20 μm/s. The red dashed circle represents a region-of-convergence for the MTB of 10 μm diameter.

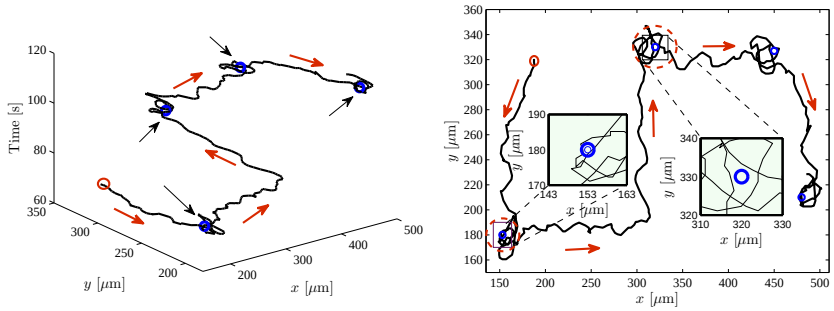

(a) Closed-loop tracking (b) MTB path

Fig. 10 Closed-loop control of the Magnetotactic Bacterium (MTB) under the influence of the magnetic fields in the absence of a field-with-alternating-direction. The black line represents the actual trajectory taken by the MTB, whereas the red arrows represent its direction. The red and blue circles indicate the initial position and the reference set-points, respectively. The entries of the diagonal controller gain matrices ($\mathbf{K}_1$) and ($\mathbf{K}_2$) are 15.0 and 15.5, respectively. (a) Motion of the MTB towards reference set-points (indicated by the black arrows). (b) The insets indicate the effect of the closed-loop control on the motion of the MTB at the first and second reference set-points. The closed-loop control action locates the MTB within the vicinity of the given reference set-points. The average velocity of the MTB is 29 μm/s. The red dashed circles represent circular regions-of-convergence for the MTB around the first and second reference set-points with diameter of 20 μm and 26 μm, respectively.

self-propulsion, closed-loop control can locate the MTB within the vicinity of the reference set-point but cannot achieve asymptotic convergence of the tracking error. As shown in Fig. 10(b), the region-of-convergence for the first and second set-points has diameter of 20 μm and 26 μm, respectively.

4 Discussion

In view of the practical limitations on the generation of magnetic field gradients, controlling the velocity of the MTB by exerting a pulling magnetic force cannot be achieved. This force (2.6×10^{-17} N for characterized magnetic dipole moment and field gradient of 4.34×10^{-16} A.m^2 and 60 mT/m, respectively) is five orders-of-magnitude less than the force generated by the MTB flagellum (2×10^{-12} N). Frequency response of MTB shows that its average velocity decreases by 38% at field frequency of 30 rad/s. This observation allows for devising a strategy to decrease the velocity of the MTB, by alternating the direction of the field lines at this frequency. In addition, characterization of the magnetic dipole moment and frequency response are used in the realization of the closed-loop control strategy. This strategy requires inducing a field-with-alternating-direction along with the fields generated by the closed-loop control laws (9), (10) and (11). The closed-loop control system

allows for positioning the MTB within the vicinity of a reference set-point along with decreasing its velocity. The closed-loop control system is further evaluated in the presence and absence of the field-with-alternating-direction. The closed-loop control system decreases the region-of-convergence and the velocity of the MTB in the presence of the field-with-alternating-direction as opposed to the same controller without this field.

4.1 Future work

Future work should include accurate characterization of the MTB frequency response over a wider frequency range. A three-dimensional magnetic system with automatic auto-focusing is essential in studying and controlling the MTB since it escapes into the third-dimension frequently. Therefore, our magnetic system will be redesigned to allow for visual tracking and control of the MTB in three-dimensional space. In addition, closed-loop control of a swarm of magnetotactic bacteria will be achieved.

4.2 Conclusions

A closed-loop control strategy for MTB is demonstrated experimentally. This strategy is based on characterizing the magnetic dipole moment and the frequency response of MTB. The characterized magnetic dipole moment using non-motile technique (*flip-time*) and motile techniques (*rotating-field* and *u-turn*) agrees with the result of the TEM images. Response of the MTB to a field-with-alternating-direction at different frequencies shows that its velocity decreases by 38 % at field frequency of 30 rad/s. These characterization results allows for devising a closed-loop control strategy based on generating two superimposed fields. The first is generated based on the position and velocity tracking errors of the MTB, whereas the second is a field-with-alternating-direction at frequency of 30 rad/s. These fields are superimposed and achieves position tracking of the MTB with a region-of-convergence of 10 μm diameter and an average velocity of 20 μm/s.

References

1. B. J. Nelson, I. K. Kaliakatsos, and J. J. Abbott: Microrobots for minimally invasive medicine. *Annual Reviews of Biomedical Engineering*, 12, 55–85, August 2010.
2. M. P. Kummer, J. J. Abbott, B. E. Kartochvil, R. Borer, A. Sengul, and B. J. Nelson: OctoMag: an electromagnetic system for 5-DOF wireless micromanipulation. *IEEE Transactions on Robotics*. 26(6), 1006–1017, December 2010.

3. S. Martel, C. C. Tremblay, S. Ngakeng, and G. Langlois: Controlled manipulation and actuation of micro-objects with magnetotactic bacteria. *Applied Physics Letters*. 89(23), 1–3, December 2006.
4. L. Dong and B. J. Nelson: Tutorial - Robotics in the small part II: nanorobotics. *IEEE Robotics and Automation Magazine*, 14(3), 111–121, September 2007.
5. A. A. Solovev, Y. Mei, E. B. Urena, G. Huang, and O. G. Schmidt: Catalytic microtubular jet engines self-propelled by accumulated gas bubbles. *Small*, 5(14), 1688–1692, April 2009.
6. R. Blackemore: Magnetotactic bacteria. *Science*, 190(4212), 377–379, October 1975.
7. D. Faivre and D. Schuler: Magnetotactic Bacteria and Magnetosomes. *Chemical Reviews*, 108(11), 4875–4898, October 2008.
8. A. S. Bahaj and P. A. B. James: Characterisation of magnetotactic bacteria using image processing techniques. *IEEE Transactions on Magnetics*. 29(6), 3358–3360, November 1993.
9. S. Martel and M. Mohammadi: Using a swarm of self-propelled natural microrobots in the form of flagellated bacteria to perform complex micro-assembly tasks. In *Proceedings of the IEEE International Conference on Robotics and Automation (ICRA)*. 500–505, Alaska, USA, May 2010.
10. S. Martel, M. Mohammadi, O. Felfoul, Z. Lu, and P. Pouponneau: Flagellated magnetotactic bacteria as controlled MRI-trackable propulsion and steering systems for medical nanorobots operating in the human microvasculature. *International Journal of Robotics Research*. 28(4), 571–582, November 2009.
11. A. S. Bahaj, P. A. B. James, and F. D. Moeschler: An alternative method for the estimation of the magnetic moment of non-spherical magnetotactic bacteria. *IEEE Transactions on Magnetics*. 32(5), 5133–5135, September 1996.
12. B. Steinberger, N. Petersen, H. Petermann, and D. G. Wiess: Movement of magnetic bacteria in time-varying magnetic fields. *Journal of Fluid Mechanics*. 273, 189–211, February 1994.
13. B. Behkam and M. Sitti: Design Methodology for Biomimetic Propulsion of Miniature Swimming Robots. *ASME Journal of Dynamic Systems, Measurement and Control*. 128, 36–43, March 2006.
14. Y. R. Chemla, H. L. Grossman, T. S. Lee, J. Clarke, M. Adamkiewicz, and B. B. Buchanan: A new study of bacterial motion: superconducting quantum interference device microscopy of magnetotactic bacteria. *Biophysical Journal*. 76(6), 3323–3330, June 1999.
15. J. D. Keuning, J. de Vries, L. Abelmann, and S. Misra: Image-based magnetic control of paramagnetic microparticles in water. In *Proceedings of the IEEE International Conference of Robotics and Systems*. 421–426, San Francisco, USA, September 2011.
16. L. E. Bertani, J. Weko, K. V. Phillips, R. F. Gray, and J. L. Kirschvink: Physical and genetic characterization of the genome of Magnetospirillum magnetotacticum, strain MS-1. *International Journal on Genes and Genomes*. 264, 257–263, January 2001.
17. K. Erglis, V. Ose, A. Zeltins, A. Sharipo, P. A. Janmey, and A. Cebers: Dynamics of magnetotactic bacteria in a rotating magnetic field. *Biophysical Journal*. 93(4), 1402–1412, August 2007.
18. D. M. S. Esquivel and H. G. P. Lins de Barros: Motion of magnetotactic microorganisms. *Journal of Experimental Biology*. 121, 153–163, September 1986.